JACS
JOURNAL OF THE AMERICAN CHEMICAL SOCIETY
Article
pubs.acs.org/JACS

Nonadiabatic Dynamics of Positive Charge during Photocatalytic Water Splitting on GaN(10-10) Surface: Charge Localization Governs Splitting Efficiency

Alexey V. Akimov,[†,‡] James T. Muckerman,[‡] and Oleg V. Prezhdo*[,†]

[†]Department of Chemistry, University of Rochester, Rochester, New York 14627, United States
[‡]Chemistry Department, Brookhaven National Laboratory, Upton, New York 11973, United States

Supporting Information

ABSTRACT: Photochemical water splitting is a promising avenue to sustainable, clean energy and fuel production. Gallium nitride (GaN) and its solid solutions are excellent photocatalytic materials; however, the efficiency of the process is low on pure GaN, and cocatalysts are required to increase the yields. We present the first time-domain theoretical study of the initial steps of photocatalytic water splitting on a GaN surface. Our state-of-the-art simulation technique, combining nonadiabatic molecular dynamics and time-dependent density functional theory, allows us to characterize the mechanisms and time scales of the evolution of the photogenerated positive charge (hole) and the subsequent proton transfer at the GaN/water interface. The calculations show that the hole loses its excess energy within 100 fs and localizes primarily on the nitrogen atoms of the GaN surface, initiating a sequence of proton-transfer events from the surface N−H group to the nearby OH groups and bulk water molecules. Water splitting requires hole localization on oxygen rather than nitrogen, necessitating nonadiabatic transitions uphill in energy on pure GaN. Such transitions happen rarely, resulting in low yields of the photocatalytic water splitting observed experimentally. We conclude that efficient cocatalysts should favor localization of the photogenerated hole on oxygen-containing species at the semiconductor/water interface.

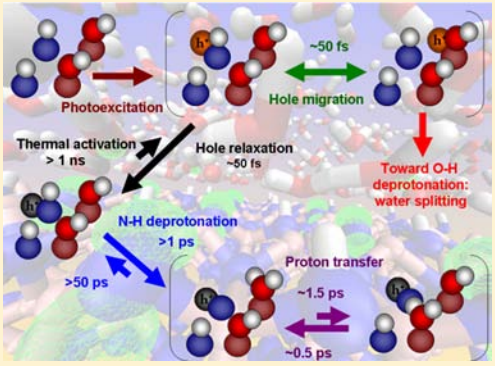

1. INTRODUCTION

Photocatalytic water splitting is a process of chemical decomposition of water driven by the energy of light, most often solar radiation. It constitutes an essential part of photosynthesis that occurs in nature.[1−3] In technological applications, the reaction requires an appropriate catalytic material. The catalysis can be either homogeneous[4,5] or heterogeneous.[4,6−9] In the latter case, the material is usually a nanoparticulate semiconductor with a band gap suitable for absorption of photons in the visible range of the solar spectrum. Further, the conduction band (CB) or valence band (VB) edges of the catalyst should be aligned appropriately for driving the hydrogen or oxygen evolution reactions (HER or OER), respectively.

Since the discovery of photocatalytic water splitting on TiO_2 electrodes by Fujishima and Honda,[10,11] significant progress has been made in the experimental characterization and preparation of various photocatalytic materials,[12−19] as well as in the theoretical description of the underlying processes and their mechanisms.[20−36] Nonetheless, the fundamental understanding is far from being complete. One of the manifestations of the lack of comprehensive knowledge underlying the principles behind photocatalytic water splitting is a relatively small quantum yield of this reaction achieved with the currently available materials. The maximal efficiency of about 6%[9,37] is achieved in the optimized $Rh_{2-y}Cr_yO_3$-loaded $(Ga_{1-x}Zn_x)$-$(N_{1-x}O_x)$. Yet, the efficiency is under 1% for most materials.[15,16,19]

The search for new efficient and cheap catalytic materials has led scientists to explore a large variety of semiconductor photocatalysts.[4,6,9,13,38−43] Among them, metal oxides[26,27,44,45] and oxinitrides[19,46] are most popular. The latter can be considered as either partially oxidized nitrides,[47] as N-doped oxides,[48] or as oxide−nitride solid solutions.[19] In recent studies Maeda and Domen have shown that pure GaN can also be used for water splitting under ultraviolet light irradiation,[49,50] although with a relatively small yield. The yield increases in a GaN:ZnO solid solution[19,46] and especially in the presence of a cocatalyst.[37]

Several authors have investigated water splitting on the nonpolar (10-10) surface of GaN theoretically.[31,51−53] They have found that adsorption of water on the GaN surface is dissociative: The hydroxide ions attach to the Ga sites, and the protons cap the nitrogen sites. Recent studies have shown that not all nitrogen sites on the GaN surface are capped with a hydrogen and that some Ga sites are coordinated with physisorbed, nondissociated water.[53] Once the hydroxyl species

Received: March 22, 2013
Published: May 16, 2013

   dx.doi.org/10.1021/ja4029395 | J. Am. Chem. Soc. 2013, 135, 8682−8691

are formed, they can participate in the molecular transformations involved in the OER, eqs 1−4:

$$S{-}OH^- + h^+ \rightarrow S{-}O^{\bullet -} + H^+ \quad (1)$$

$$S{-}O^{\bullet -} + H_2O + h^+ \rightarrow S{-}OOH^- + H^+ \quad (2)$$

$$S{-}OOH + h^+ \rightarrow S{-}O_2^{\bullet} + H^+ \quad (3)$$

$$S{-}O_2^{\bullet} + H_2O + h^+ \rightarrow S{-}OH + O_2^{\bullet\bullet} + H^+ \quad (4)$$

Here, S represents surface. The energies of all steps have been computed, showing that removal of the proton from the chemisorbed OH group, eq 1, is the rate-limiting step, requiring about 60 kcal/mol.[51] A similar conclusion has been drawn for the water splitting process on TiO_2 surfaces.[22,24]

Because the first step, eq 1, is rate limiting, it is very important to understand the factors affecting its kinetics. Particularly, the dynamics of the photogenerated hole, h^+, involved in this process must be taken into account. In this work, we present the first time-domain ab initio study of the initial steps of water splitting at the GaN(10-10)/water interface. Using our nonadiabatic molecular dynamics (NA-MD) approach formulated within the framework of time-dependent density functional theory (TD-DFT), we obtain valuable insights into the relaxation and migration of the photogenerated hole as well as the subsequent proton-transfer processes (Figure 1). The calculations allow us to formulate a comprehensive kinetic model of the interfacial dynamics involving charge and proton transfer. A detailed analysis of the photoinduced transformations enables us to identify the key factors affecting both the initial, rate-limiting step, eq 1, and the final, recovery step, eq 4, of the photocatalytic cycle.

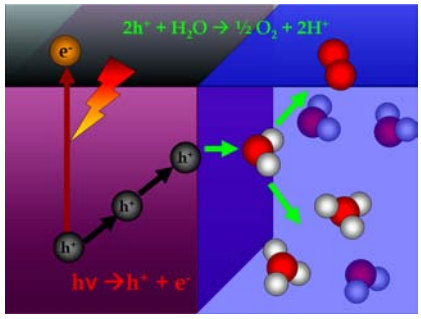

Figure 1. Schematic representation of processes involved in the heterogeneous water oxidation process.

Our calculations show that the photogenerated hole relaxes to the edge of the GaN VB within 100 fs. Once the hole arrives at the surface, it localizes primarily on the nitrogen atoms and induces proton migration from the N atom on the surface to a nearby adsorbed hydroxyl ion, effectively converting it to H_2O. Proton transfer between the newly formed H_2O and nearby OH species, as well as proton migration to bulk water, follow. Only rarely the photogenerated hole localizes on oxygen-containing species, as required by eq 1, contributing to the low efficiency of photocatalytic water splitting on the pure GaN surface, observed experimentally. These findings allow us to conclude that efficient cocatalysts should favor hole localization on oxygen-containing species adsorbed on the catalyst surface.

The following section details the theoretical and computational methodology used to model the photoinduced chemical dynamics at the GaN/water interface. The Results and Discussion section is divided into subsections focusing on the electronic structure of the interface before and after the photoexcitation, the nonadiabatic relaxation of the photogenerated hole, the transient hole delocalization onto water, and the sequence of photoinduced proton-transfer steps following the hole relaxation. The paper concludes with formulation of a comprehensive kinetic scheme of the initial steps involved in the photocatalytic water splitting and a summary of the key findings.

2. THEORETICAL METHODOLOGY

In order to study the initial steps of the photocatalytic water splitting on the GaN surface, shown schematically in Figure 1, we perform ab initio electronic structure and MD calculations, followed by NA-MD simulations. We consider the two states of the photocatalytic system: The "off" state represents the system before the photon is absorbed, and the "on" state describes the situation after the photogenerated hole is created. We assume that the excited electron is separated from the hole spatially: A photon is absorbed, and the electron and hole are generated in bulk GaN. Then, the hole travels to the GaN/water interface, while the electron moves toward a hydrogen evolution site or another reaction center. The analysis of the electronic structure and dynamic properties of the neutral ("off" state) and charged

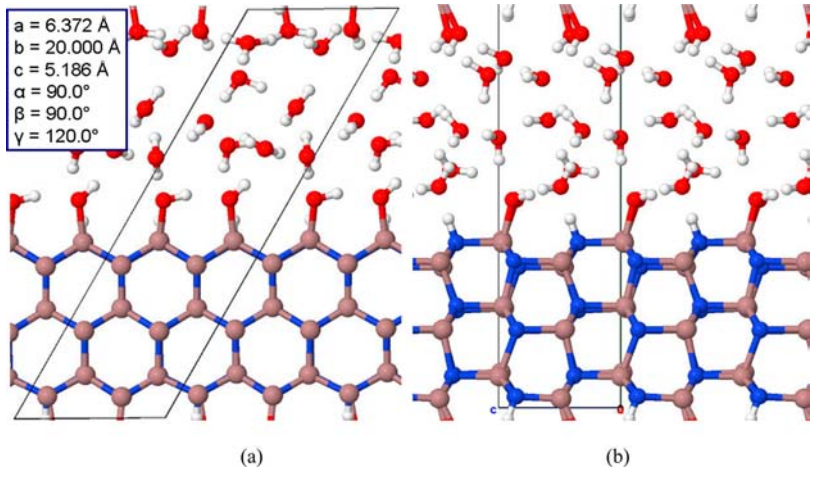

Figure 2. Simulation cell with its periodic images: (a) front and (b) side views.

dx.doi.org/10.1021/ja4029395 | J. Am. Chem. Soc. 2013, 135, 8682−8691

("on" state) systems assists us in characterizing the effects of the photoexcitation and the subsequent nuclear dynamics on the initial steps of the photocatalytic water splitting. The details of the simulation procedure are given in the following subsections.

2.1. Ab Initio Electronic Structure and MD. The molecular structure of the studied system is presented in Figure 2. The simulation involves 60 atoms per unit cell, including a GaN semiconductor slab and 12 water molecules dispersed in the region between the surface layer and its periodic image, corresponding approximately to the water density of 1.0 g/cm^3. Such choice of the simulation cell, along with the appropriately selected setup for the electronic structure calculation, provides the best compromise between the accuracy of the system representation and the computational cost, allowing trajectories as long as 50 ps to be computed within reasonable time by ab initio MD.

The geometry optimization, electronic structure, and adiabatic MD calculations were performed with the Quantum Espresso program,[54] utilizing a converged plane wave basis and a pseudopotential representation of the core electrons. In particular, the ultrasoft pseudopotential generated within the Perdew–Burke–Ernzerhof (PBE) generalized gradient approximation (GGA) was used.[55,56] Stipulated by the size of the molecular system and the pseudopotential, the simulation cell of the neutral system contained 312 explicit electrons, including d-electrons of Ga atoms. As has been shown previously,[53] d-electrons of Ga are important for correct description of the electronic structure of GaN. The size of the plane wave basis was chosen to satisfy the 30 Ry energy cutoff. The calculations performed on the system with the hole employed Gaussian smearing of the orbital populations with the 0.005 Ry smearing width. The smearing is usually required for the spin-polarized calculations of the charged systems to avoid the problems with convergence. However, the width of the smearing is relatively small, and the results are not affected significantly, as ascertained by additional calculations with varying smearing constant. The initially optimized structure formed the starting point for the adiabatic (Born–Oppenheimer) MD calculations. A 50 ps trajectory was computed for the neutral system, representing the interface prior to the photoexcitation. The Verlet[57] integration algorithm with 1 fs time step was used. The Andersen[58] thermostat was employed to maintain ambient temperature. The initial conditions for the NA-MD simulations were sampled from the 50 ps adiabatic trajectory, as described in the following subsection. The molecular structures, and the charge and spin densities were visualized and analyzed using the VMD[59] and J-ICE[60] programs.

2.2. Nonadiabatic MD. In order to model relaxation of the photogenerated hole, it is crucial to employ a methodology that is capable of describing spontaneous transitions between different electronic states. Extensions of MD to include such transitions are known as NA-MD. Trajectory surface hopping (TSH)[61,62] provides one of the most common means to perform NA-MD. The time-dependent Schrodinger equation $i\hbar\partial|\Psi\rangle/\partial t = H|\Psi\rangle$ is solved along the nuclear trajectory $R(t)$. The probability of electronic transitions between states $|i\rangle$ and $|j\rangle$ is then determined from the time-dependent amplitudes $\{c_i(t)\}$ of a basis set representation in the total wave function, $|\Psi(t,R)\rangle = \sum_i c_i(t)|i(R)\rangle$ and from the magnitude of the nonadiabatic coupling $d_{ij} = \langle i|d/(dt)|j\rangle$. The current simulations employed the adiabatic basis, $\{|i\rangle\}$. A detailed description of the NA-MD algorithm used,[61,63] its implementation within the TD-DFT framework,[64,65] and general discussion of the NA-MD methodology[66−70] can be found elsewhere. NA-MD proved extremely useful in studies of various processes, where the NA effects come into play. In particular, the TD-DFT/NA-MD methodology developed and implemented in the Prezhdo group[64] has been used to study the electron transfer in dye-sensitized semiconductor solar cells,[71,72] the electron−phonon relaxation dynamics in quantum dots,[73−75] carbon nanotubes,[76] and other nanoscale systems,[77,78] Auger-type processes[74] and related phenomena.

The basis states $\{|i(R)\rangle\}$ of the photogenerated hole were selected as a set of Kohn–Sham (KS) orbitals within some energy range near the GaN VB edge. In particular, we chose the energy window of about 2.5 eV below the HOMO, including 30 outermost occupied KS orbitals. The NA couplings were computed numerically, using the approximation:[79]

$$d_{ij}(t+dt) \approx \frac{1}{2dt}[\langle i(t)|j(t+dt)\rangle - \langle i(t+dt)|j(t)\rangle] \tag{5}$$

The average magnitude of the NA couplings between all pairs of adjacent states:

$$d_{\mathrm{adj}}^{(1)} = \frac{1}{T\cdot N}\sum_i |d_{i,i+1}| \tag{6}$$

is estimated from our calculations to be $d_{\mathrm{adj}}^{(1)} = 67.90$ meV. The averaging is performed over N trajectories of duration T each.

To perform the NA-MD simulation we computed 20 nonequilibrium trajectories, starting at random configurations from the 50 ps adiabatic MD trajectory. Thus, all starting points corresponded to the equilibrium configurations of the system prior to the photoexcitation. Assuming that the photogenerated hole migrates toward the GaN/water interface while the electron moves to another reaction site, e.g., a hydrogen evolution center, and that the electronic structure of the system responds instantaneously to hole generation, the system was charged at $t = 0$, and the NA-MD simulations were performed using the adiabatic KS orbital basis for the charged system. The positive charge was compensated by the uniformly distributed charge density of the opposite sign. The nonequilibrium NA-MD trajectories were 1 ps in length. 200 independent stochastic realizations of the TSH algorithm were obtained along each trajectory, resulting in 4000 evolutions total and providing sufficient statistical convergence for the computed properties.

In our calculations, we assume that the photogenerated electron−hole pair rapidly dissociates. This allows us to neglect the electron−hole interaction, which requires significantly more expensive computational methods to be used. Such an approximation is well justified, since it is known for many semiconductor materials that photoexcitation yields charge carriers separated over a large spatial extent. The electron−hole interaction may be important during the photoexcitation process, when the charge carriers are produced. In our simulations, we do not consider photoexcitation explicitly and assume that charge carrier separation has completed.

2.3. Analysis of the Proton-Transfer Dynamics. In order to analyze the proton-transfer dynamics, which follow relaxation of the photogenerated hole inside the GaN VB and hole localization on the surface, we developed a generic methodology to define automatically the reaction coordinate for proton transfer in a complex environment. In the previous studies of the proton-transfer dynamics,[53,80,81] the reaction coordinate was typically defined by projecting the O−H vector

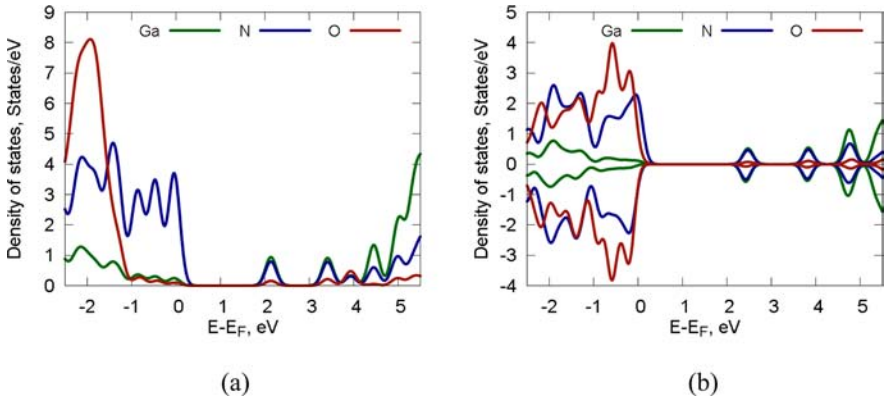

Figure 3. Projected densities of states for (a) neutral and (b) charged (+1.0) simulation cells. The Fermi energy, E_F, is set equal to the energy of the HOMO orbital.

onto the O−O vector, formed by the two oxygen atoms between which the hydrogen is transferred. If the H atom is closer to one of the O atoms, the state corresponds to the "reactant" configuration, while if the H atom is closer to the other O atom, the state corresponds to the "product" configuration. However, such procedure requires an a priori definition of the reactant and product states, and it is hard to apply to complex reaction coordinates involving more than three atoms.

In our methodology, described in detail in section B of Supporting Information, we define molecular states on the basis of the coordination numbers of all atoms in the system. The number of atoms located within a certain tolerance distance of a given atom defines its coordination number. The coordination numbers of all atoms in the system form a vector with integer components. The vector labels the molecular state. This methodology has the following advantages: (1) It is applicable to polyatomic systems with complex reaction coordinates. A subset of atomic species can be used to simplify or enhance the analysis. (2) There is no need for an a priori definition of states. Such definition constitutes a nontrivial problem in general. (3) New states can be automatically discovered along an MD trajectory.

The tolerance distance is the only adjustable parameter. A physically reasonable value for the parameter can be chosen, for instance, based on the van der Waals or covalent radii of the atoms involved. In our simulations, all hydrogen atoms located closer than 1.355 Å to an oxygen atom contribute to the oxygen coordination number. For simplicity, we focused on H atoms coordinated to O atoms and did not consider O−O or H−H coordination. A small variation of the tolerance distance did not affect the results, proving robustness of the method.

Analysis of molecular states along MD trajectories provides important information about the system and its dynamics. It identifies the key states involved in the nuclear dynamics, including both minima and transition states. The probability of observing each state can be used to evaluate the state free energy:

$$\Delta F_i = -k_B T \ln(p_i) \tag{7}$$

By computing the average mean free passage times between the states, one estimates the rates of the corresponding transitions.

3. RESULTS AND DISCUSSION

Our study indicates that the early events induced at the GaN/water interface by photoexcitation occur in the following sequence. Creation of an electron−hole pair causes reorganization of the electronic structure of the interface. Then, the hole loses energy by coupling to phonons and relaxes to the edge of the GaN VB. Transiently during the relaxation process the hole can hop onto the oxygen atoms of hydroxyl group and interfacial water molecules, facilitating the first photochemical reaction, eq 1. Ultimately, at the end of the charge-phonon relaxation, the hole localizes on the N atoms of the surface, initiating a sequence of proton-transfer events starting with the proton attached to the N atoms and involving nearby surface OH groups and water molecules. With small probability, the hole can be thermally activated onto an oxygen atom, catalyzing the dissociation of the O−H bond and leading to formation of the S−O species, eq 1. It should be noted that these mechanistically distinct steps can overlap in time, as discussed below.

3.1. Electronic Structure of the GaN/Water Interface.

The analysis of the electronic structure by means of the projected density of states (pDOS) provides important information about the types of orbitals and species involved in the hole relaxation, localization, and transfer processes. The computed pDOS for the neutral and charged systems are presented in Figure 3. The result for the neutral system, describing the GaN/water interface prior to photoexcitation, is in good agreement with the previous calculations.[53] The computed electronic band gap for the GaN subsystem is around 2.0 eV, which is notably smaller than the experimental value of 3.4 eV. This well-known shortcoming of pure DFT functionals stems from the electron self-interaction problem. It can be corrected by hybrid functionals and other techniques, which however make the computational cost of NA-MD prohibitive. The absolute value of the electronic band gap is irrelevant for the present study, since the study focuses on the positive charge evolving exclusively within the VB manifold.

The atomic analysis shows that the main contributions to all frontier VB orbitals of the GaN/water interface arise from the 2p orbitals of N and O atoms. The contributions from the d orbitals of Ga atoms and s orbitals of all atomic species are insignificant. For the neutral system, Figure 3a, the energy of the 2p orbitals of the O species lies lower than the energy of the 2p orbitals localized on the N species. In a hypothetical case of the hole occupying the orbitals obtained for the neutral species,

dx.doi.org/10.1021/ja4029395 | J. Am. Chem. Soc. 2013, 135, 8682−8691

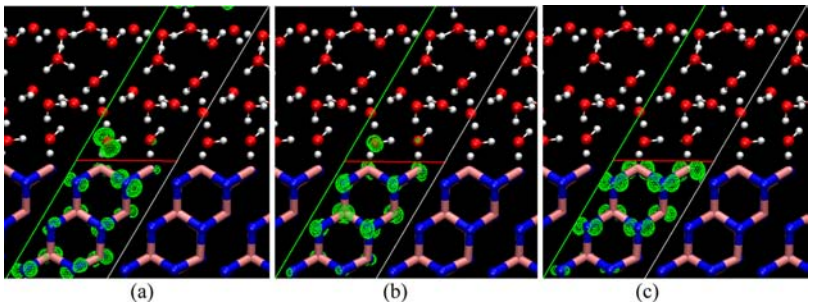

Figure 4. Electron spin-density of the charged system at various energies below the VB edge: (a) E_h = 0.22 eV; (b) E_h = 0.06 eV; (c) E_h = 0.0 eV. The spin-density isovalue is equal to 0.0025 au. The spin-density indicates the spatial location of the hole.

the energy of the hole would be significantly smaller if it were localized on the N species than on the O species. Note that the hole energy increases as it moves away from the VB edge. If the hole is prepared deeper in the VB, e.g., at energies 1−2 eV below the edge, where a significant contribution from the O atoms is present, it will eventually migrate to the N atoms, where its energy is minimal. The back-transfer of the hole from the N orbitals to the O orbitals is possible in principle, but it is inhibited significantly by the Boltzmann factor, because the energy difference between the VB edge dominated by the N orbitals and the onset of the O orbital contributions to the VB is rather large, about 1.0 eV (Figure 3a). For reference, k_BT = 0.025 eV at room temperature. According to the hypothetical scenario based on the band structure of the neutral system, the hole will effectively be trapped by the N sites, preventing water oxidation, which requires hole localization on surface hydroxyl groups and adsorbed water molecules, eq 1.

Upon photoexcitation, the hole migrates to the GaN/water interface, while the electron moves to another spatial part of the system. The local region of the semiconductor around the hole becomes positively charged. The pDOS for the charged system is presented in Figure 3b. Note that the charged system carries a spin of 1/2, and therefore, Figure 3b presents pDOS for spin-up and spin-down orbitals. One can observe a significant change in the atomic origin of the orbitals near the VB edge. Although the HOMO is still localized on the N atoms, orbitals as close as 0.1 eV in energy to the HOMO attain contributions from the O atoms. Therefore, thermally activated nonadiabatic transitions from the lower-lying N states to the O states become much more likely. In a realistic system carrying positive charge near the interface, there exists a considerable chance of hole localization on the O species, making the photoinduced water oxidation on the GaN surface feasible both thermodynamically and kinetically.

In addition to the pDOS analysis presented above, it is instructive to visualize hole localization on frontier orbitals. For this purpose, we compute spin-density of the charged system for different hole excitation energies (Figure 4). The spin-density indicates the spatial location of the hole. As follows from the pDOS shown in Figure 3 and illustrated in Figure 4, for the moderate hole energies accessible by solar photons, the hole states are supported by the overlapping 2p orbitals of the O and N atoms. The hole created in GaN migrates toward the surface, simultaneously losing energy to vibrations and relaxing to the HOMO state. The partitioning of the hole between the N and O species depends on its energy. At higher energies, the hole is partially delocalized on the O species (Figure 4a,b). As the hole loses energy and relaxes to its lowest state, the fraction of the hole density supported by the OH groups decreases, and the hole localizes on the N atoms of the GaN substrate (Figure 4c).

We note that the current study is performed using a pure DFT functional, since it provides the computational efficiency needed to perform the TD-DFT/NA-MD simulations in the extended surface system. Pure DFT functionals exhibit the electron self-interaction error[82,83] and tend to favor delocalized electronic state densities. The error can be reduced with hybrid functionals; however, they are significantly more computationally demanding in periodic calculations. In order to put our study on a firmer theoretical ground, we performed single point electronic structure calculations with the hybrid PBE0 functional (Supporting Information, section A). This increased the spacing between the electronic energy levels, and the GaN band gap in particular; nevertheless, the hole in its lowest energy state remained localized on the N atoms of the GaN surface. The performed tests support the validity of our calculations.

Hybrid functionals were used previously by Shen et al.[51] in water oxidation studies with cluster models. In contrast to the present results, the cluster approach predicted preferential localization of the hole on the OH groups chemisorbed on the GaN surface. It should be noted that cluster models may artificially favor hole localization due to finite size of the system. Further, for computational efficiency, Shen et al. used different pseudopotentials for the bulk and surface atoms, creating an asymmetry in the description of the surface and bulk regions, possibly also increasing hole localization. By employing periodic boundary conditions and the same level of theory for the bulk and surface regions, the present work eliminated these issues.

In general, as has been shown by Finazzi et al.[84] with periodic TiO_2 calculations, charge localization is quite sensitive to the details of the method employed: Hybrid functionals can produce delocalized states; energetically close localized and delocalized states can be obtained. Apart from the approximations used in the electronic structure calculations, one may need to account for zero-point vibrational energy,[85−87] which is neglected in most studies including the present work, as well as for NA effects, which are included in our work for the first time.

Regardless of the approximations and possible complications discussed above, the photoinduced reaction dynamics can be represented as a two-step process: (1) energy relaxation and migration of the photogenerated hole from GaN onto O species, such as surface hydroxyl groups and molecular water; and (2) chemical reactions induced by the hole and involving proton transfer, eq 1. In the next subsections, we provide detailed description of these two processes.

3.2. Nonadiabatic Relaxation of the Photogenerated Hole. The kinetics of the hole energy relaxation is presented in

dx.doi.org/10.1021/ja4029395 | J. Am. Chem. Soc. 2013, 135, 8682−8691

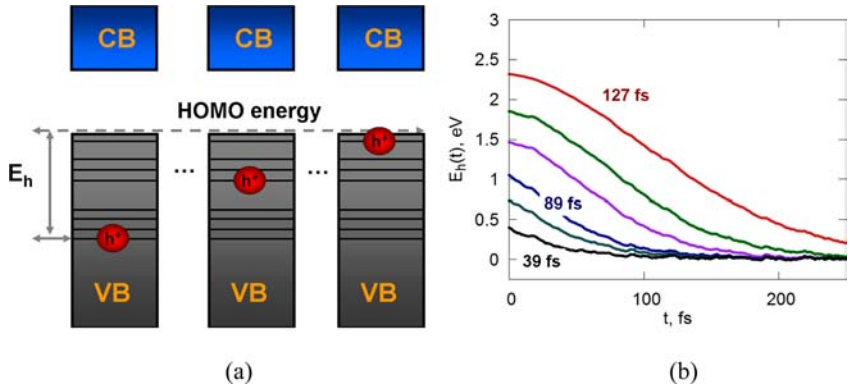

Figure 5. Relaxation of the photogenerated hole by coupling to vibrational motions of the atoms. (a) Schematic of the relaxation process. The hole energy is defined relative to the HOMO energy. Deeper VB states correspond to higher hole energies. (b) Results of the nonequilibrium nonadiabatic simulations for different initial energies of the hole.

Figure 5. As schematically denoted in Figure 5a, the hole is initially prepared in the GaN VB at a certain energy E_h. The hole energy E_h is defined as the difference between the energies of the HOMO and the orbital on which the hole resides at a specific time. This quantity is minimal (0.0 eV) when the hole is completely relaxed to the HOMO. During the relaxation process, the average energy of the hole is a time-dependent quantity, which can be measured directly in experiment. We computed this quantity as a function of time for a range of initial hole excitation energies (Figure 5b).

Figure 5b shows that the decay law of the hole energy relaxation changes from exponential for small initial energies (black to dark-blue lines) to Gaussian for larger excitation energies (violet to dark-red lines). The characteristic relaxation times are obtained by fitting of the computed curves to the corresponding decay law. The decay times vary in the range from 40 to 130 fs, depending on the initial excitation energy. The simulations show that the hole relaxes to its lowest energy state of the ultrafast time scale, which is shorter than the time scale of the majority of chemical reactions.

The evolution of the photogenerated hole can proceed through two different mechanisms: (1) hot hole diffusion driven by the potential gradient near the surface, followed by nonadiabatic relaxation; (2) nonadiabatic relaxation of the photogenerated hole, followed by the diffusion. As suggested by our NA-MD calculations, the time-scale of the hot hole relaxation is on the order of 100 fs. In a large system, electrons and holes are generated in the bulk region, far away from the surface, and the hole needs a significantly longer time to travel to the surface than to relax. Thus, the mechanism, in which the hole relaxes down in energy first and then diffuses to the surface, driven by the surface states that form the VB edge, is most feasible. In reality, both processes proceed in parallel, and one may need alternative approaches and larger model systems to fully account for possible effects that arise from such complex dynamics.

3.3. Transient Delocalization of the Hole onto Water.

As the hole relaxes down in energy by coupling to vibrational motions and reaches the edge of the VB, it can move between GaN and water. Since hole localization on the O species is a prerequisite for the first step of the water splitting process, eq 1, hole transfer onto water during the nonadiabatic relaxation deserves investigation. Figure 6 illustrates such process for a sample trajectory.

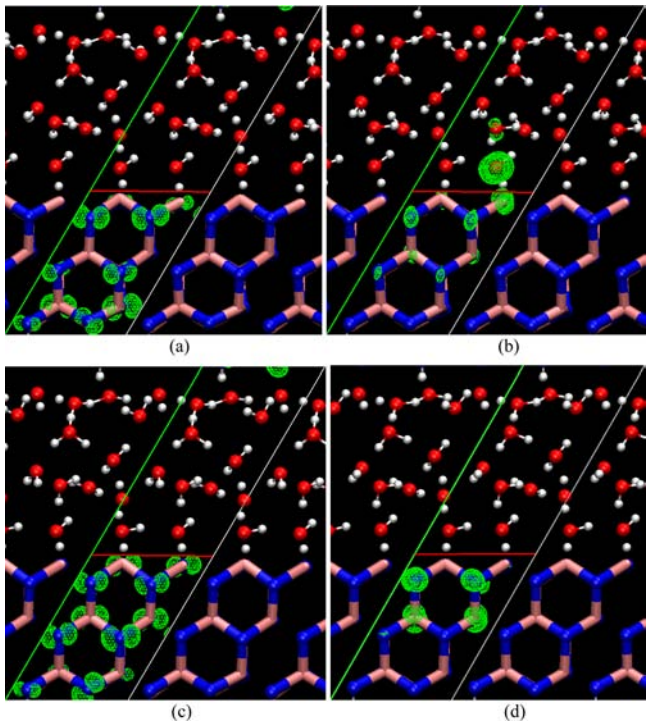

Figure 6. Electron spin density along a relaxation trajectory: (a) E_h = 0.22 eV, t = 0 fs; (b) E_h = 0.06 eV, t = 50 fs; (c) E_h = 0.0 eV, t = 100 fs; and (d) E_h = 0.0 eV, t > 100 fs. The spin-density isovalue is equal to 0.0025 au. The spin density indicates the spatial location of the hole.

On a 50 fs time scale, i.e., about once during the nonadiabatic relaxation, the hole moves from GaN to water. This allows the hole to dwell for some time on the surface-bound hydroxyl ions and to initiate photochemical events. It should be emphasized that the hole delocalization onto oxygen species discussed in this subsection happens while the hole is still "hot", that is, before it has relaxed to the VB edge. At higher energies, the states supporting the hole arise from the hybridized 2p orbitals of the O and N atoms (Figure 3). While the hole is still hot, it contains a contribution from the 2p orbitals of oxygens, which varies in time depending on nuclear motion. Since the hole relaxation process is extremely fast (Figure 5) and is generally shorter than the time scale of nuclear reorganization, the system should already exist in a suitable nuclear configuration for the reaction to occur. Otherwise, the hole will relax to its lowest

dx.doi.org/10.1021/ja4029395 | J. Am. Chem. Soc. 2013, 135, 8682−8691

energy state and move back onto GaN, not causing any chemical transformation. Since the likelihood of the appropriate nuclear motion, making the photochemical reaction take place on a 100 fs time scale, is rather small, the efficiency of the water oxidation on the GaN surface is low. This agrees well with the experimental findings.[18,46]

It is important to emphasize the significance of the relaxation time scale, obtained in this work, in drawing conclusions regarding the small water oxidation efficiency. Under the conditions, in which the N levels are energetically more favorable than the O levels, the ultrafast hole relaxation dynamics deteriorates the water splitting efficiency. If the hole relaxation were slow, then the time spent by the hole on the O-containing species would be sufficiently long to induce the O−H dissociation, despite the fact that the hole populated the O-containing species only transiently. Thus, a simple static picture, drawn on the basis of the energy of hole states localized on different parts of the system, provides only a partial insight into the mechanism of the water splitting reaction. In addition to the thermodynamic feasibility, the kinetic time scales, such as those obtained with the NA-MD method employed in this work, are needed for a comprehensive characterization of the process. The kinetic aspects become particularly important for nonequilibrium phenomena initiated by light.

After the photogenerated hole has relaxed to its energy minimum, it can be thermally excited into higher energy states delocalized onto the O species. The energy difference between the hole ground state and the VB states with contributions from the O atoms is on the order of 0.1 eV (Figure 3b). The probability of thermal activation is given by the Boltzmann factor, which is on the order of 0.02 at room temperature. This value represents an upper estimate for the fraction of photogenerated holes delocalized onto water. A more accurate estimate can be obtained by multiplying this number by the localization of these states on the O atoms. The fraction is rather small for the pure GaN surface; however, it can be increased in other materials, in which the energy difference between the hole ground state and the states localized on OH groups is comparable to the thermal energy. In particular, this is likely the case for systems employing oxides and oxinitrides as cocatalysts.[19,50] An ideal photocatalytic material for water oxidation should be engineered in a way to make the ground state of the hole localized primarily on the O-containing species and not on the substrate. These conjectures require more detailed studies and will be the subject of our future work.

3.4. Photoinduced Proton-Transfer Events. Our study indicates that the most stable configuration of the neutral system corresponds to the GaN (10-10) surface with all N atoms passivated by dissociated water molecules (Figure 7a). This stable configuration was maintained for the whole duration of the 50 ps trajectory produced in our work. Less stable configurations with the GaN surface containing unpassivated N atoms represent local energy minima. These states transform to the most stable configuration on a 5 ps time scale. The above results rationalize why the initial proton-transfer reaction, eq 1, is very unlikely, and water is not oxidized in the neutral system.

The situation is reversed in the charged system: The configuration with the uncapped surface nitrogen (Figure 7b) is most stable. The proton detaches from the N atom and reacts with the OH group to form a water molecule. In our simulation, only one of the four surface N−H groups loses the proton. This number is determined by the number of holes

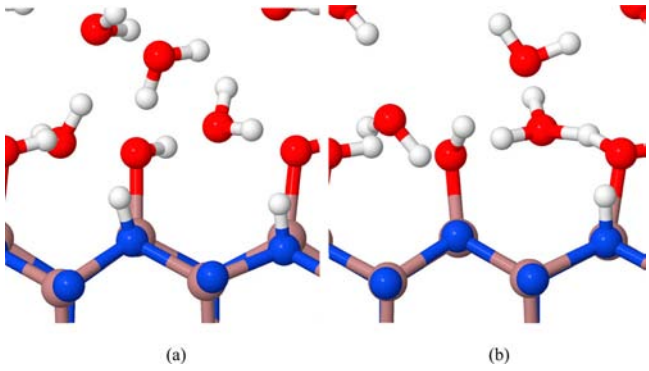

Figure 7. Representative configurations corresponding to the most stable states of the (a) neutral and (b) charged systems.

residing on the surface. In the ideal situation of a relatively low surface density of the holes, it can be assumed that each hole releases one proton, as in eq 1. For higher surface hole concentrations, the yield is expected to decrease, because some of the holes will be pushed away from the surface by electrostatic interactions. In realistic systems, the surface density of the holes is relatively low, because many of the photogenerated holes recombine with the electrons before they can reach the surface.

It is quite interesting that the Ga atom connected to the uncapped nitrogen carries the OH group rather than the full water molecule, as one could intuitively expect. The latter is coordinated to a Ga site adjacent to a capped N site. The intuitively expected configuration is an energetically close local minimum. These configurations are related by proton transfer via the bridging water molecule, as illustrated in Figure 8.

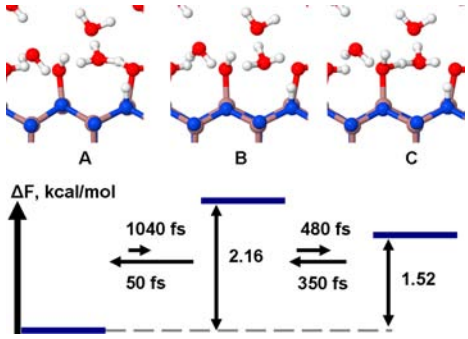

Figure 8. Proton-transfer reaction at the GaN/water interface in the charged system. The vertical black arrow represents the free energy axis, the horizontal blue lines represent the free energy of the molecular configurations (states) denoted as A−C in the panel above.

The free energies of the most stable states of water on the positively charged GaN (10-10) surface are presented in Figure 8. Figure 8A shows the lowest energy configuration with physisorbed water molecule attached to the Ga atom that is a second nearest neighbor to the uncapped N atom. Figure 8C shows the second lowest energy configuration, with the physisorbed water molecule bound to Ga that is nearest to the uncapped N. Figure 8B shows the transition state containing the H_3O^+ cation. The free energy of B characterizes the barrier for the proton transfer between states A and C. The free energy barriers are 2.16 kcal/mol for the A→C transition and 0.64 kcal/mol for the C→A transition. The time of the proton transfer from A to C is about 1.6 ps and is equal to the

dx.doi.org/10.1021/ja4029395 | J. Am. Chem. Soc. 2013, 135, 8682−8691

sum of the times for A→B and B→C. The proton-transfer times are calculated as the mean free passage times. Both the free energy barriers and the transition times are in good agreement with the experimental studies[88,89] as well as with the other theoretical works.[53,80]

The algorithm described in the Analysis of the Proton-Transfer Dynamics section has automatically discovered a few other metastable states in the charged system. Such configurations arise from proton delocalization between H_2O−Ga and OH−Ga centers via an intermediate water molecule, similarly to the state shown in Figure 8B. The additional metastable states arise from the one depicted in Figure 8B by nuclear rearrangements of surrounding water molecules not shown in the figure. Further, in the case of the charged slab, it is possible to observe a metastable state, in which the proton is transferred into the bulk-like water layer. Such state appears and disappears quite often with the mean free passage time of 98 fs for the forward transition and 22 fs for reverse transition. The states with the proton transferred into the bulk-like water layer are higher in energy than those shown in Figure 8. Thus, the proton is more likely to transfer among the hydroxyl groups along the surface rather than diffuse into bulk water.

It is worth noting that in configurations with uncapped N atoms (Figure 7b), the hole localizes strongly on the nitrogens, and the O levels move inside the VB considerably, in comparison to the fully passivated system. The detailed studies of the pDOS for such configurations are described in Supporting Information, section A. Thus, we observe a positive feedback: Hole migration toward the surface induces deprotonation of a surface N−H site, while such deprotonation favors hole localization on the created free-N surface site, preventing further hole migration to the O-containing species. This result suggests that the water oxidation efficiency can be improved by chemically modifying the surface to minimize deprotonation of the N−H sites.

4. CONCLUSIONS

We studied the ultrafast processes that follow the photogeneration of a positive charge at the GaN/water interface and constitute the initial steps of the water oxidation reaction. Using an ab initio NA-MD approach, we characterized the quantum dynamics of hole relaxation, mediated by coupling to nuclear vibrations, the hole transfer from GaN to water, and the ensuing proton-transfer events. Our calculations show that the hole relaxes to its lowest energy state on a 100 fs time scale. In this state, the hole is localized on the nitrogen atoms of the substrate surface. During the energy relaxation, the hole transiently populates the oxygen species, making the water oxidation process possible from both kinetic and thermodynamics points of view. The relaxation kinetics of the hole determines its dwelling time on the surface hydroxyl groups, and this time is about 50 fs and is too short in general, to initiate the nuclear rearrangements required for the water oxidation reaction, contributing to low efficiency of water splitting on pure GaN. In order to achieve efficient water oxidation, the photogenerated hole should localize on the hydroxyl groups of water dissociatively adsorbed on the substrate surface. The goal can be achieved experimentally either by O-containing cocatalysts on pure GaN or by other substrates, such as oxinitrides.

We found that in the absence of a hole, water molecules are completely dissociated, occupying all Ga and N surface sites available. The situation is qualitatively different for the charged surface, where some protons dissociate from the surface N−H groups and migrate near the surface. We developed a simple and robust algorithm to discover automatically the states involved in complex equilibria in large systems and applied it to study the proton-transfer reactions taking place at the GaN/water interface. We found that the hole induces deprotonation of the surface N−H groups. The result is a hydroxonium cation and a free, uncapped N site. The proton moves further between the hydroxonium and the adjacent chemisorbed hydroxyl groups or, with a smaller probability, diffuses into bulk water. We calculated the free energy barriers for the proton transfer along the GaN surface are 2.16 and 0.64 kcal/mol, depending on the direction of the proton transfer among the asymmetric surface sites. The characteristic time of the proton-transfer reaction starting from the most stable configuration of the charged surface is estimated as 1.6 ps. Both the free energy barriers and the transfer rates are in good agreement with the available experimental and theoretical studies.

Finally, based on the first-principles calculations, we constructed a comprehensive kinetic model of the processes taking place during the initial stages of the photoinduced water oxidation reaction on the GaN(10-10) surface (Figure 9). The detailed analysis of both nonequilibrium and quasi-equilibrium processes reported in this work improves our understanding of the fundamental principles underlying operation of photocatalytic systems and suggests criteria for rational design of better photocatalytic materials. In particular, our study strongly indicates that an efficient material for water oxidation should favor hole localization on surface hydroxyl groups. Lacking in pure GaN, this feature can be achieved with composite materials, such as oxide cocatalysts, oxinitride substrates, and their chemically modified derivatives.

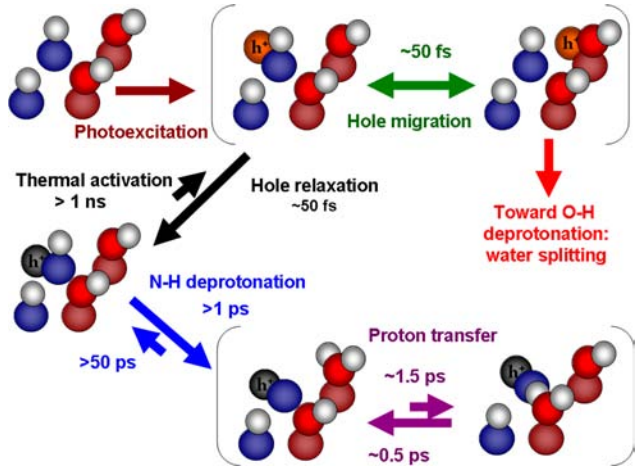

Figure 9. Kinetic scheme of the hole and proton migration processes involved in the initial stages of the photocatalytic water oxidation.

■ ASSOCIATED CONTENT

Supporting Information

Calculations illustrating the effects of simulation cell size, DFT functional, and surface N protonation on hole localization; detailed description of the state-finding algorithm for proton-transfer dynamics. This material is available free of charge via the Internet at http://pubs.acs.org.

dx.doi.org/10.1021/ja4029395 | J. Am. Chem. Soc. 2013, 135, 8682−8691

AUTHOR INFORMATION

Corresponding Author

oleg.prezhdo@rochester.edu

Notes

The authors declare no competing financial interest.

ACKNOWLEDGMENTS

Authors thank the members of the Solar Water Splitting Simulation Team (SWaSSiT) group for useful discussions and comments on the work. A.V.A. was funded by the Computational Materials and Chemical Sciences Network (CMCSN) project at Brookhaven National Laboratory under contract DE-AC02-98CH10886 with the U.S. Department of Energy and supported by its Division of Chemical Sciences, Geosciences & Biosciences, Office of Basic Energy Sciences. O.V.P. acknowledges financial support of the U.S. Department of Energy, grant DE-SC0006527.

REFERENCES

(1) McEvoy, J. P.; Brudvig, G. W. *Chem. Rev.* **2006**, *106*, 4455−4483.
(2) Enns, K.; Burgess, W. H. *J. Am. Chem. Soc.* **1965**, *87*, 1822−1823.
(3) Rossmeisl, J.; Dimitrievski, K.; Siegbahn, P.; Norskov, J. K. *J. Phys. Chem. C* **2007**, *111*, 18821−18823.
(4) Walter, M. G.; Warren, E. L.; McKone, J. R.; Boettcher, S. W.; Mi, Q.; Santori, E. A.; Lewis, N. S. *Chem. Rev.* **2010**, *110*, 6446−6473.
(5) McCool, N. S.; Robinson, D. M.; Sheats, J. E.; Dismukes, G. C. *J. Am. Chem. Soc.* **2011**, *133*, 11446−11449.
(6) Kudo, A.; Miseki, Y. *Chem. Soc. Rev.* **2009**, *38*, 253.
(7) Osterloh, F. E.; Parkinson, B. A. *MRS Bull.* **2011**, *36*, 17−22.
(8) Teoh, W. Y.; Scott, J. A.; Amal, R. *J. Phys. Chem. Lett.* **2012**, *3*, 629−639.
(9) Kubacka, A.; Fernández-García, M.; Colón, G. *Chem. Rev.* **2012**, *112*, 1555−1614.
(10) Fujishima, A.; Honda, K. *Bull. Chem. Soc. Jpn.* **1971**, *44*, 1148−1150.
(11) Fujishima, A.; Honda, K. *Nature* **1972**, *238*, 37.
(12) Yamakata, A.; Yoshida, M.; Kubota, J.; Osawa, M.; Domen, K. *J. Am. Chem. Soc.* **2011**, *133*, 11351−11357.
(13) Ni, M.; Leung, M. K. H.; Leung, D. Y. C.; Sumathy, K. *Renew. Sust. Energ. Rev.* **2007**, *11*, 401−425.
(14) Yu, H.; Irie, H.; Hashimoto, K. *J. Am. Chem. Soc.* **2010**, *132*, 6898−6899.
(15) Ishikawa, A.; Takata, T.; Kondo, J. N.; Hara, M.; Kobayashi, H.; Domen, K. *J. Am. Chem. Soc.* **2002**, *124*, 13547−13553.
(16) Hisatomi, T.; Maeda, K.; Takanabe, K.; Kubota, J.; Domen, K. *J. Phys. Chem. C* **2009**, *113*, 21458−21466.
(17) Woodhouse, M.; Parkinson, B. A. *Chem. Soc. Rev.* **2009**, *38*, 197.
(18) Maeda, K.; Domen, K. *J. Phys. Chem. Lett.* **2010**, *1*, 2655−2661.
(19) Ohno, T.; Bai, L.; Hisatomi, T.; Maeda, K.; Domen, K. *J. Am. Chem. Soc.* **2012**, *134*, 8254−8259.
(20) Haussener, S.; Xiang, C.; Spurgeon, J. M.; Ardo, S.; Lewis, N. S.; Weber, A. Z. *Energy Environ. Sci.* **2012**, *5*, 9922−9935.
(21) Zipoli, F.; Car, R.; Cohen, M. H.; Selloni, A. *J. Am. Chem. Soc.* **2010**, *132*, 8593−8601.
(22) Valdés, A.; Qu, Z.-W.; Kroes, G.-J.; Rossmeisl, J.; Nørskov, J. K. *J. Phys. Chem. C* **2008**, *112*, 9872−9879.
(23) Valdés, A.; Kroes, G.-J. *J. Chem. Phys.* **2009**, *130*, 114701.
(24) Valdés, A.; Kroes, G.-J. *J. Phys. Chem. C* **2010**, *114*, 1701−1708.
(25) Hellman, A.; Pala, R. G. S. *J. Phys. Chem. C* **2011**, *115*, 12901−12907.
(26) Xu, H.; Zhang, R. Q.; Ng, A. M. C.; Djurišić, A. B.; Chan, H. T.; Chan, W. K.; Tong, S. Y. *J. Phys. Chem. C* **2011**, *115*, 19710−19715.
(27) Inoue, Y. *Energy Environ. Sci.* **2009**, *2*, 364.
(28) Vojvodic, A.; Norskov, J. K. *Science* **2011**, *334*, 1355−1356.
(29) Sobolewski, A. L.; Domcke, W. *J. Phys. Chem. A* **2008**, *112*, 7311−7313.
(30) Wang, F.; Di Valentin, C.; Pacchioni, G. *J. Phys. Chem. C* **2012**, *116*, 8901−8909.
(31) Chen, P.-T.; Sun, C.-L.; Hayashi, M. *J. Phys. Chem. C* **2010**, *114*, 18228−18232.
(32) Livraghi, S.; Paganini, M. C.; Giamello, E.; Selloni, A.; Di Valentin, C.; Pacchioni, G. *J. Am. Chem. Soc.* **2006**, *128*, 15666−15671.
(33) Ardo, S.; Meyer, G. J. *J. Am. Chem. Soc.* **2010**, *132*, 9283−9285.
(34) Jensen, S.; Kilin, D. *Int. J. Quantum Chem.* **2012**, *112*, 3874.
(35) Zhang, Y.; Kilin, D. *Int. J. Quantum Chem.* **2012**, *112*, 3867.
(36) Badaeva, E.; Isborn, C. M.; Feng, Y.; Ochsenbein, S. T.; Gamelin, D. R.; Li, X. *J. Phys. Chem. C* **2009**, *113*, 8710−8717.
(37) Hisatomi, T.; Minegishi, T.; Domen, K. *Bull. Chem. Soc. Jpn.* **2012**, *85*, 647−655.
(38) Fujishima, A.; Rao, T. N.; Tryk, D. A. *J. Photochem. Photobiol., C* **2000**, *1*, 1−21.
(39) Ardo, S.; Meyer, G. J. *Chem. Soc. Rev.* **2009**, *38*, 115.
(40) Osgood, R. *Chem. Rev.* **2006**, *106*, 4379−4401.
(41) Chen, X.; Mao, S. S. *Chem. Rev.* **2007**, *107*, 2891−2959.
(42) Smestad, G. P.; Steinfeld, A. *Ind. Eng. Chem. Res.* **2012**, *51*, 11828−11840.
(43) Thompson, T. L.; Yates, J. T. *Chem. Rev.* **2006**, *106*, 4428−4453.
(44) Nozik, A. J. *Nature* **1975**, *257*, 383−386.
(45) Giordano, L.; Pacchioni, G. *Acc. Chem. Res.* **2011**, *44*, 1244−1252.
(46) Maeda, K.; Takata, T.; Hara, M.; Saito, N.; Inoue, Y.; Kobayashi, H.; Domen, K. *J. Am. Chem. Soc.* **2005**, *127*, 8286−8287.
(47) Smith, W.; Fakhouri, H.; Pulpytel, J.; Mori, S.; Grilli, R.; Baker, M. A.; Arefi-Khonsari, F. *J. Phys. Chem. C* **2012**, *116*, 15855−15866.
(48) Reyes-Gil, K. R.; Reyes-Garcia, E. A.; Raftery, D. *J. Phys. Chem. C* **2007**, *111*, 14579−14588.
(49) Ryu, S.-W.; Zhang, Y.; Leung, B.; Yerino, C.; Han, J. *Semicond. Sci. Technol.* **2012**, *27*, 015014.
(50) Maeda, K.; Teramura, K.; Lu, D.; Takata, T.; Saito, N.; Inoue, Y.; Domen, K. *Nature* **2006**, *440*, 295−295.
(51) Shen, X.; Small, Y. A.; Wang, J.; Allen, P. B.; Fernandez-Serra, M. V.; Hybertsen, M. S.; Muckerman, J. T. *J. Phys. Chem. C* **2010**, *114*, 13695−13704.
(52) Shen, X.; Allen, P. B.; Hybertsen, M. S.; Muckerman, J. T. *J. Phys. Chem. C* **2009**, *113*, 3365−3368.
(53) Wang, J.; Pedroza, L. S.; Poissier, A.; Fernández-Serra, M. V. *J. Phys. Chem. C* **2012**, *116*, 14382−14389.
(54) Gianozzi, P.; Baroni, S.; Bonini, N.; Calandra, M.; Car, R.; Cavazzoni, C.; Ceresoli, D.; Chiarotti, G. L.; Cococcioni, M.; Dabo, I.; Dal Corso, A.; De Gironcoli, S.; Fabris, S.; Fratesi, G.; Gebauer, R.; Gerstmann, U.; Gougoussis, C.; Kokalj, A.; Lazzeri, M.; Martin-Samos, L.; Marzari, N.; Mauri, F.; Mazzarello, R.; Paolini, S.; Pasquarello, A.; Paulatto, L.; Sbraccia, C.; Scandolo, S.; Sclauzero, G.; Seitsonen, A. P.; Smogunov, A.; Umari, P.; Wentzcovitch, R. M. *J. Phys.: Condens. Matter* **2009**, *21*, 395592.
(55) Perdew, J. P.; Burke, K.; Ernzerhof, M. *Phys. Rev. Lett.* **1996**, *77*, 3865−3868.
(56) Perdew, J. P.; Burke, K.; Ernzerhof, Matthias *Phys. Rev. Lett.* **1997**, *78*, 1396.
(57) Verlet, L. *Phys. Rev.* **1967**, *159*, 98−103.
(58) Andersen, H. C. *J. Chem. Phys.* **1980**, *72*, 2384−2393.
(59) Humphrey, W.; Dalke, A.; Schulten, K. *J. Mol. Graphics* **1996**, *14*, 33−38.
(60) Canepa, P.; Hanson, R. M.; Ugliengo, P.; Alfredsson, M. *J. Appl. Crystallogr.* **2011**, *44*, 225−229.
(61) Tully, J. C. *J. Chem. Phys.* **1990**, *93*, 1061−1071.
(62) Sholl, D. S.; Tully, J. C. *J. Chem. Phys.* **1998**, *109*, 7702.
(63) Fabiano, E.; Keal, T. W.; Thiel, W. *Chem. Phys.* **2008**, *349*, 334−347.
(64) Craig, C.; Duncan, W.; Prezhdo, O. *Phys. Rev. Lett.* **2005**, *95*, 163001.
(65) Isborn, C. M.; Li, X. *J. Chem. Theory Comput.* **2009**, *5*, 2415−2419.

(66) Hack, M. D.; Truhlar, D. G. *J. Phys. Chem. A* **2000**, *104*, 7917−7926.
(67) Hack, M. D.; Wensmann, A. M.; Truhlar, D. G.; Ben-Nun, M.; Martínez, T. J. *J. Chem. Phys.* **2001**, *115*, 1172.
(68) Drukker, K. *J. Comput. Phys.* **1999**, *153*, 225−272.
(69) Li, X.; Tully, J. C.; Schlegel, H. B.; Frisch, M. J. *J. Chem. Phys.* **2005**, *123*, 084106.
(70) Fischer, S. A.; Chapman, C. T.; Li, X. *J. Chem. Phys.* **2011**, *135*, 144102.
(71) Duncan, W. R.; Stier, W. M.; Prezhdo, O. V. *J. Am. Chem. Soc.* **2005**, *127*, 7941−7951.
(72) Stier, W.; Duncan, W. R.; Prezhdo, O. V. *Adv. Mater.* **2004**, *16*, 240−244.
(73) Neukirch, A. J.; Guo, Z.; Prezhdo, O. V. *J. Phys. Chem. C* **2012**, *116*, 15034−15040.
(74) Madrid, A. B.; Hyeon-Deuk, K.; Habenicht, B. F.; Prezhdo, O. V. *ACS nano* **2009**, *3*, 2487−2494.
(75) Hyeon-Deuk, K.; Prezhdo, O. V. *Nano Lett.* **2011**, *11*, 1845−1850.
(76) Habenicht, B.; Craig, C.; Prezhdo, O. *Phys. Rev. Lett.* **2006**, *96*, 187401.
(77) Long, R.; Prezhdo, O. V. *J. Am. Chem. Soc.* **2011**, *133*, 19240−19249.
(78) Long, R.; English, N. J.; Prezhdo, O. V. *J. Am. Chem. Soc.* **2012**, *134*, 14238−14248.
(79) Hammes-Schiffer, S.; Tully, J. C. *J. Chem. Phys.* **1994**, *101*, 4657.
(80) Zahn, D.; Brickmann, J. *Chem. Phys. Lett.* **2000**, *331*, 224−228.
(81) Zahn, D. *J. Chem. Theory Comput.* **2006**, *2*, 107−114.
(82) Dreuw, A.; Head-Gordon, M. *J. Am. Chem. Soc.* **2004**, *126*, 4007−4016.
(83) Prezhdo, O. V. *Adv. Mater.* **2002**, *14*, 597.
(84) Finazzi, E.; Di Valentin, C.; Pacchioni, G.; Selloni, A. *J. Chem. Phys.* **2008**, *129*, 154113.
(85) Espinosa-García, J.; Corchado, J. C.; Truhlar, D. G. *J. Am. Chem. Soc.* **1997**, *119*, 9891−9896.
(86) Billeter, S. R.; Webb, S. P.; Agarwal, P. K.; Iordanov, T.; Hammes-Schiffer, S. *J. Am. Chem. Soc.* **2001**, *123*, 11262−11272.
(87) Sebastianelli, F.; Xu, M.; Bačić, Z.; Lawler, R.; Turro, N. J. *J. Am. Chem. Soc.* **2010**, *132*, 9826−9832.
(88) Agmon, N. *Chem. Phys. Lett.* **1995**, *244*, 456−462.
(89) Meiboom, S. *J. Chem. Phys.* **1961**, *34*, 375.